

A Multi-functional Inspection Robot for Civil Infrastructure Evaluation and Maintenance

Spencer Gibb, Tuan Le, Hung Manh La, *Senior Member, IEEE*, Ryan Schmid, and Tony Berendsen.

Abstract—Satisfactory operation of civil infrastructure is of critical importance to an economy. In order to maintain performance, infrastructure needs to be properly maintained. Inspecting infrastructure is inherently labor-intensive work and costly. In this paper, we propose a solution to cost-effective infrastructure inspection by developing a multi-functional inspection robot. The robot is equipped with several state-of-the-art non-destructive evaluation (NDE) sensors to perform inspection. The robot is able to perform selected inspection methods in certain areas based on multiple sensor data fusion. With this, the overall inspection time is reduced, which in turn reduces maintenance cost. An inspection framework based on multiple NDE data sensor fusion is proposed. Detailed discussions include robot design, robot navigation and sensor data fusion.

I. INTRODUCTION

Maintenance of civil infrastructure plays a crucial part in guaranteeing the healthy economic growth and social development of a modern society. According to [1], there are several infrastructure sectors critical to the economic prosperity of the United States, including aviation, ports, bridges, and roads. Naturally, all civil infrastructures are subject to deterioration, which gradually leads to complete deficiency without proper maintenance. It is projected that infrastructure deficiency will cost the US GDP a sum of \$3.9 trillion US by 2025 [1]. In order to prevent this catastrophe, one must act on two fronts: invest to build new infrastructures and maintain current ones. Maintaining the condition of current infrastructure is more cost-effective than building new infrastructure. Multiple maintenance programs for infrastructure have been researched and developed [2]. In our previous work [3]–[6], we pointed out that proper infrastructure (bridge) inspection for maintenance is labor-intensive work, which inspired several efforts to automate inspection processes and replace human operators to reduce maintenance costs and work related injuries due to the unsafe working conditions of civil infrastructure inspection jobs.

In this paper, we develop a multi-functional autonomous inspection robot, which is capable of operating in both indoor

and outdoor environments. Participating in the National Science Foundation (NSF) Innovation Corps (I-Corps™) 2015 program, we discovered that infrastructure owners desire minimal interruption to normal operations while infrastructure inspection is being performed. Hence, we develop an inspection framework based on multi-sensor fusion, in which our robot can reduce inspection time by choosing fast or in-depth inspection mode for a particular area judging by equipped non-destructive evaluation (NDE) sensors [7], [8]. A set of NDE sensors, including ground-penetrating radar (GPR) for concrete rebar assessment [9], electrical resistivity (ER) for concrete corrosion assessment, and stereo camera for crack detection, is integrated into the robot. The data processing software for these NDE sensors are developed and implemented on the robot's on-board computers to allow the robot to inspect the infrastructure in real-time. For navigation, the robot also employs an inertial measurement unit (IMU) in conjunction with a global positioning system (GPS) receiver and a stereo camera. Our robot has two complementary navigation capabilities: a GPS+IMU-Extended Kalman Filter (EKF) based navigation for outdoor inspections [10], [11], and a visual-inertia odometry based on stereo vision and inertial information [12] for indoor inspections. We propose and discuss a new method for fusing NDE sensor information in order for the robot to perform only necessary inspection in certain areas, and thus reduce inspection time.

The remainder of this paper is organized as follows: in section II, we shortly discuss the robot's mechanical design and the robot's navigation capabilities. Section III provides information about our NDE sensor fusion framework. In section IV, a conclusion is given and a discussion of future work is provided.

II. MECHANICAL DESIGN AND NAVIGATION

In this section, we provide a description of our robot's mechanical design in Fig. 1. The mobile base platform is a skid-steering robot from Omron Adept Robotics. A Novatel Flex6 GPS unit is located at the center of the robot above a water tank. On the front of the robot, the ER sensors, camera, and IMU are mounted, while the GPR sensor is mounted on the rear of the robot. This design and sensor mounting is based on our work in [3] with several major modifications to the lift systems for both ER and GPR deployment.

The developed robotic system handles navigation for indoor and outdoor scenarios differently. An example of the outdoor navigation can be seen in Fig. 2, where the EKF is used to fuse GPS data, data from the robot's

This work is supported by National Science Foundation under grants: NSF-IIP-I-Corps #1559942 and 1639092, the National Aeronautics and Space Administration (NASA) under Grant No. NNX10AN23H issued through the Nevada Space Grant, and the Nevada Advanced Autonomous Systems Innovation Center (NAASIC) at the University of Nevada, Reno.

Spencer Gibb, Tuan Le, Dr. Hung La and Ryan Schmid are with the Advanced Robotics and Automation (ARA) Lab, Department of Computer Science and Engineering, University of Nevada, Reno, NV, 89557, USA

Tony Berendsen is with Department of Mechanical Engineering, University of Nevada, Reno, NV, 89557, USA

The first two authors have made equal contributions to this work.

Corresponding author: Hung Manh La (e-mail: hla@unr.edu).

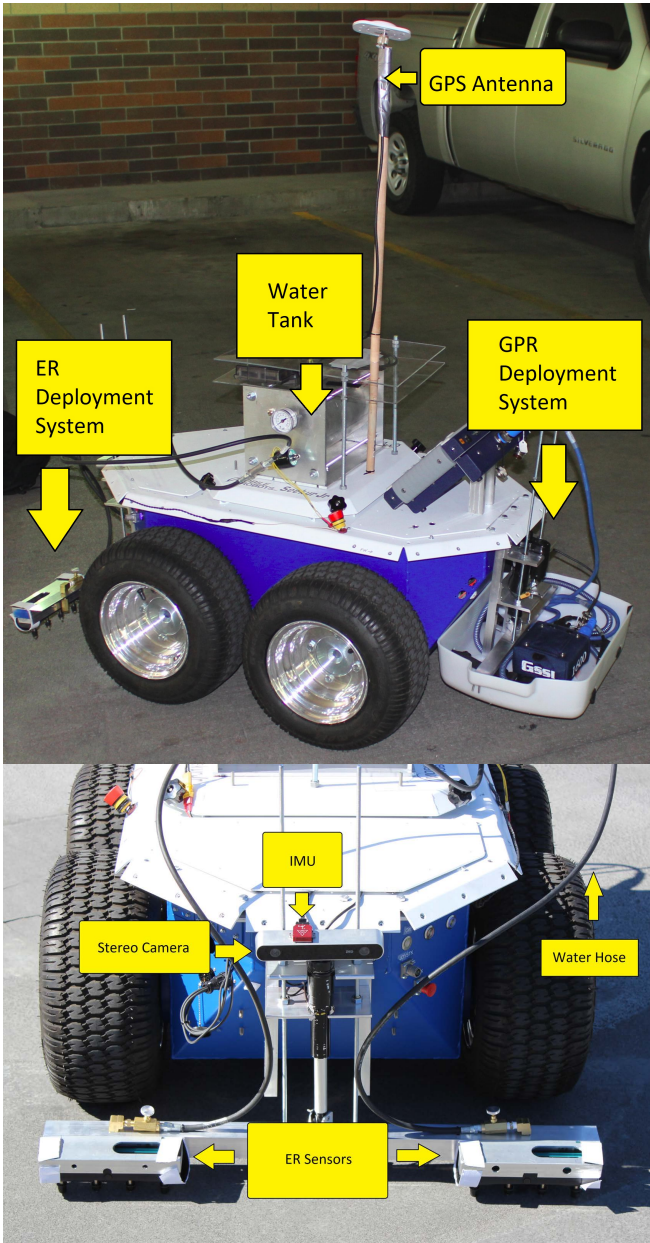


Fig. 1: An image of the entire robotic system showing the GPR deployment system, water tank, and GPS (top). A labeled image of the front of the robot, where the camera, IMU, and ER are mounted (bottom).

wheel encoder, and IMU data [13]. For indoor navigation, a technique called visual-inertial odometry-based navigation is employed, which uses the stereo camera equipped on the robot. More information on the indoor navigation method can be found in [12]. The two modes of navigation allow the developed robotic system to navigate in any environment even though GPS signal may not be available due to the inspection area being a parking garage or other large indoor structure that might block the GPS signal.

III. NON-DESTRUCTIVE EVALUATION SENSOR FUSION

In this section, we propose an inspection framework based on NDE sensor data fusion. In order to reduce inspection

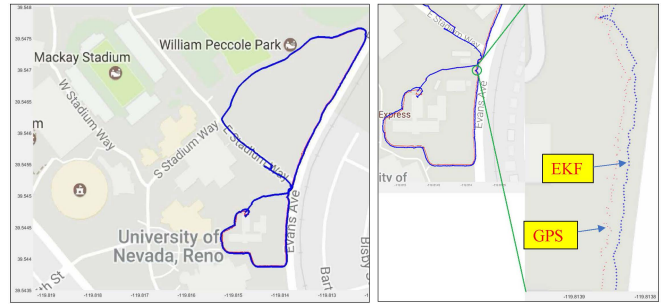


Fig. 2: (Left sub-figure) Performance of GPS+IMU-EKF-based localization with *robot_localization* package. The red dots are GPS signal and blue dots are output of EKF localization. (Right-sub figure) Zoom-in/Close-look at one location: the EKF outperforms the GPS alone since it outputs smoother results.

time, the robot needs to decide in which area it can perform a fast inspection (using less sensors) and which area requires an in-depth inspection (using all available sensors).

The robotic system developed as part of the proposed method is capable of collecting data from several sensors. Among those sensors are GPR, camera, and ER. In order to make a decision on whether to deploy the ER sensor, which is much more time consuming than the GPR sensor or camera, a sensor fusion method is developed to minimize inspection time. The proposed method is tested on two sets of data collected at the University of Nevada, Reno (UNR) campus. This process is described in the following sub-sections, where we discuss data processing and provide details about how the robot can make inspection decision based on multiple sensor data fusion.

A. Camera Data Pre-processing

The camera attached to the robotic system is used to collect visual data during the inspection process. This visual data is in the form of frames saved as images. The camera is configured to capture twenty frames per second, which are saved to one of the two on-board computers. Because of the large number of frames captured during the inspection process and the real-time nature of the proposed method, it is not realistic to attempt to process all of the images captured by the camera. Instead, a Laplacian scoring method is used to eliminate duplicate or unnecessary frames, and to ensure that all frames used for later processing are not blurry frames, which might cause issues with processing.

Laplacian scoring is accomplished by convolving each input frame by a Laplacian mask that is a discrete approximation of the Laplacian, which can be seen in Equation (1).

$$L = \begin{bmatrix} 0 & 1 & 0 \\ 1 & -4 & 1 \\ 0 & 1 & 0 \end{bmatrix} \quad (1)$$

After convolving a frame with the Laplacian mask, the variance of the frame is calculated as in Equation (2),

$$\sigma^2 = \frac{\sum(X - \mu)^2}{N} \quad (2)$$

where X is the current pixel value, μ is the mean pixel value after the Laplacian mask is applied, and N is the number of pixels in the image.

The process of Laplacian scoring yields a single number describing the frame, which can be used to eliminate blurry frames. It was empirically determined, that any frame with $\sigma^2 < 100$ was not suitable for use in later processing, whereas frames with $\sigma^2 > 300$ were typically sharp and high quality. For the proposed method, any frame with $\sigma^2 < 200$ was discarded.

Since the robotic system moves at a set speed during the data collection process, it is also safe to assume that if there are multiple sharp frames within a short time span, then all but one can be discarded since the frames capture the same area of the ground. Discarding frames this way depends on the speed of the robot and the way the camera is mounted on the robot, which affects the distance of ground covered by each image.

B. Edge Detection and the Crack Map

Once suitable frames are picked out using the pre-processing steps described in the previous section, edge detection is performed to locate cracks in the concrete surface that are present in each frame. Some advanced existing crack detection methods [14], [15] can be used. However, for the simplicity, in this paper the edge detection method used is Canny edge detection. Some details of the Canny method will be described here, and further information can be found in [16].

Each frame processed using the Canny method is first smoothed through convolution with a Gaussian filter. This smoothing process helps remove noise from the image that may affect the edge detection process. Four separate filters are then applied to the frame to get horizontal, vertical, and both diagonal directions of edges. Then the edge gradient is calculated as in Equation (3) and the direction is calculated as in Equation (4).

$$G = \sqrt{G_x^2 + G_y^2}. \quad (3)$$

$$\theta = \text{atan2}(G_y, G_x). \quad (4)$$

where, G_x is the first derivative of the smoothed image in the x direction and G_y is the first derivative of the smoothed image in the y direction.

Non-maxima suppression is then performed to thin edges in the image, leaving only the local maxima intensity values remaining in the edge image. After non-maxima suppression is performed, a double threshold technique and hysteresis are applied to the edge image to keep only strong edges.

The proposed method takes the results from the Canny method and labels all connected components in the edge image. This yields a label matrix containing all segmented edges in the image. From this matrix, the major axis for each edge in the image is calculated. The length of each major axis is used to determine the length of edges in the image and apply an edge length filter. The edge length filter removes edges that are too small and may be a result of insignificant



Fig. 3: An example image of the surveyed area (top), and an example output image from the crack detection algorithm with length filter applied (bottom).

objects in the image, while also removing edges that are extremely long and caused by the lines between concrete slabs, as can be seen in Fig. 3-Top. It was empirically determined that any edge with major axis length l is kept in the edge image if: $50 \text{ pixels} < l < 500 \text{ pixels}$. Binary images containing white edges are output by the edge detection and filtering process, which can be seen in Fig.3.

These edge images can be concatenated to produce a larger image which shows the location of all of the significant cracks in the inspected area. An example of the crack map produced by this edge detection process can be seen in Fig. 4-Top and Fig. 6-Top.

C. Ground-Penetrating Radar Pre-processing

In addition to camera data, GPR data is also collected throughout the inspection process by the robotic system developed for the proposed method. GPR produces a unique signature for each subsurface object, including steel rebar, which serve to reinforce concrete. A GPR scan image can be seen in Fig. 5. The algorithm used to locate subsurface objects in GPR scan images can be seen in [17], and has not been detailed here due to space constraints.

D. GPR Contour Mapping

Using the rebar locations from the rebar picking algorithm described previously, it is possible to generate a condition map of the inspected area. These condition maps show the condition of the inspected area based on the depth of the rebar in the inspected area. GPR condition maps are

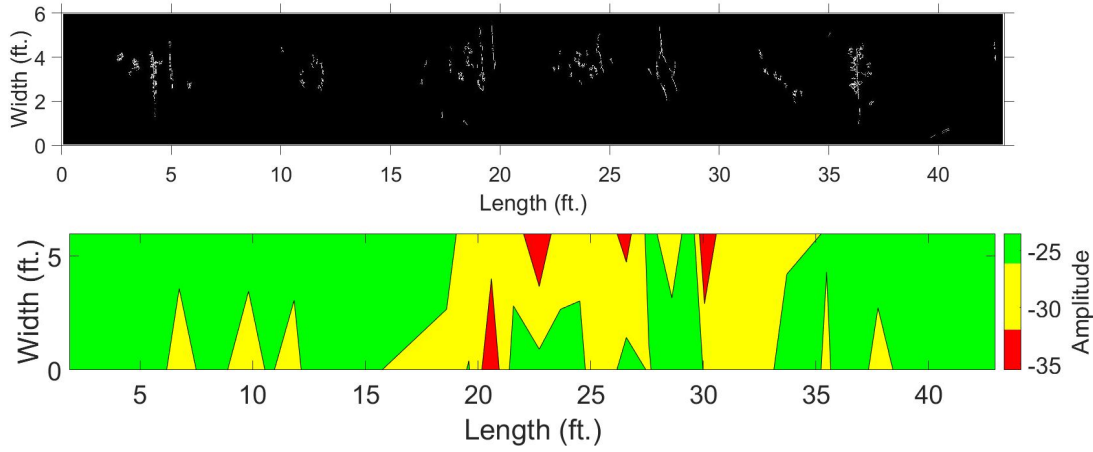


Fig. 4: (Top figure) The crack map of the camera data collected for the first part of the test data. (Bottom figure) The contour plot of the GPR data collected for the first part of the test data.

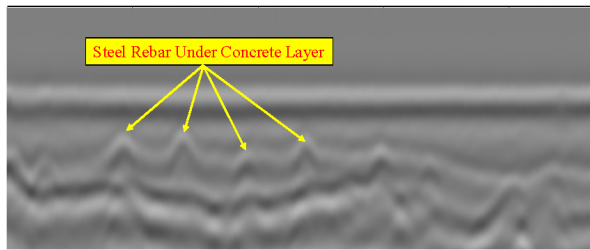


Fig. 5: An example image of the subsurface objects generated by the GPR sensor.

represented as contour plots with colors representing the condition of rebar underneath the inspected surface. As seen in Fig.4-Bottom and Fig. 6-Bottom, green areas are areas where the GPR data indicates the rebar beneath the concrete are in good condition, yellow areas are in questionable (unknown whether these areas are in good or poor condition) condition, and red areas are in poor condition.

E. Fusion and the ER Deployment Map

The primary contribution of the proposed method is that it fuses sensor data to minimize inspection time. Of the sensors on the robotic platform, three are used for inspection: the camera, GPR and the ER sensor. Of the three sensors, ER takes the most time to deploy, which means it may not be viable to deploy the ER sensor everywhere in inspection area. Through deploying the camera and GPR unit, it is possible to eliminate a majority of the inspection time that would result in using the ER sensor everywhere in the inspection area.

The crack map generated from the camera data, and the condition map generated from the GPR data can be fused into an ER deployment map so that the ER sensor is only deployed in areas where it is needed to ascertain the condition of the inspection area, and not everywhere. Sensor fusion is a technique for improving the results of data from an individual sensor through combining it with data from another sensor. This technique is used for many types of sensors and data [18]. Although GPR data for condition mapping has not been fused with camera data for crack detection, research on fusing GPR data with other sensors does exist [19], and research on fusion of other NDE sensors also exists [20], [21].

In the proposed method, sensor fusion is accomplished through use of a confidence matrix. This matrix, M_d , can be seen in Equation (5).

$$M_d = \begin{bmatrix} 0 & 0 \\ d & 0/1 \\ 0 & 0 \end{bmatrix} \quad (5)$$

Equation (5) shows the decision matrix where the first row is the case where the condition map is green in the given

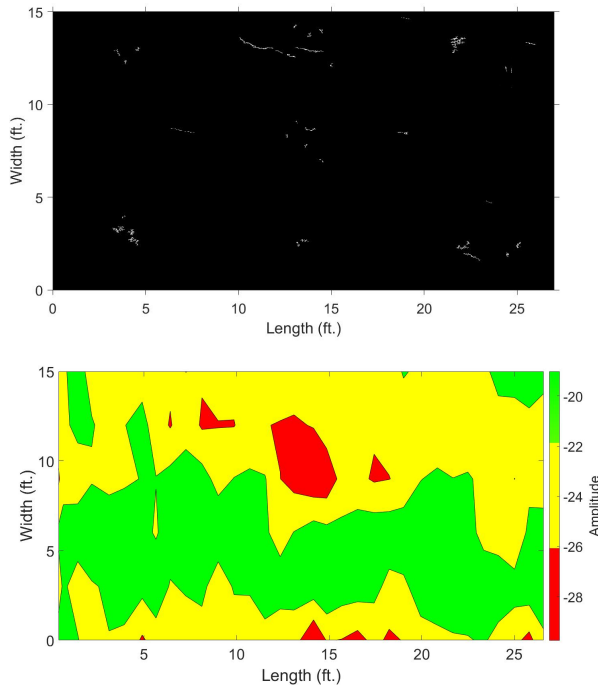


Fig. 6: (Top) The crack map of the camera data collected for the second part of the test data. (Bottom) The contour plot of the GPR data collected for the second part of the test data. There are some indications of correlation between these two maps: more cracks in the corroded areas (yellow and red color areas in the GPR map).

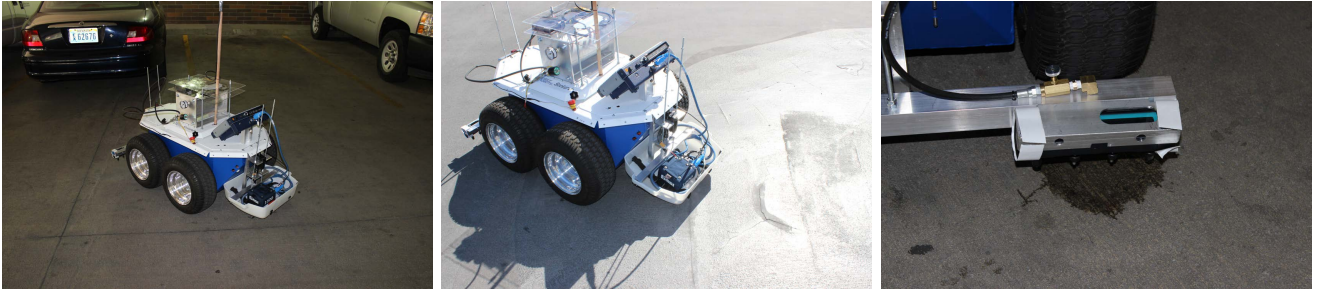


Fig. 7: Images of the robotic system being deployed for inspection of a parking garage on the University of Nevada, Reno campus (left and middle). An image of the ER sensor being deployed to measure the resistance of the concrete at the inspection site (right), where water was sprayed on the concrete to create a conductive environment to enable ER measurement.

area, the second row is the case where the condition map is yellow in the given area, and the third row is the case where the decision map is red in the given area. The first column of the decision matrix represents the case where there are cracks present in the corresponding area of the crack map, and the second column represents the case where there are no cracks present in the corresponding area of the crack map.

The explanation for the matrix in Equation (5) is that GPR serves as the primary source of information about the area that is being inspected. In the cases where the GPR data shows that the area is in good condition (green on the condition map), then crack information is not necessary, as it doesn't provide any additional certainty that the inspection area is in good or poor condition. Elements (1,1) and (1,2) in the decision matrix represent these cases. In addition, if the GPR shows that the inspection area is in poor condition, crack information is not required since the GPR provides high certainty that the inspection area needs repair and in what precise location. Elements (3,1) and (3,2) in the decision matrix represent these cases. The final cases are where the GPR data does not show conclusively what the condition of the inspection area is, which requires fusion with crack data to determine if the ER sensor should be deployed to make a final decision on the condition of the area in question. Elements (2,1) and (2,2) in the decision matrix represent these cases. In the case of element (2,2), since there are no cracks present in that area, it is not possible to use the crack information in conjunction with the GPR data, so the deploying the ER can be left up to the user. In the case of element (2,1) in the decision matrix, it is necessary to analyze the presence of cracks in the given area with respect to the surrounding area, as in Equations (6, 7, 8, 9). This decision matrix is applied across the inspection area by splitting the area into equally sized cells and making a decision on a cell by cell basis as to whether the ER sensor should be deployed. In the experiments conducted for this paper, a cell size of 1 square foot was used, but the cell size may vary based on the size of the inspection area.

$$d = \text{round}\left(\frac{\sigma_C - \mu_{IA}}{m_{IA} - \mu_{IA}}\right) \quad (6)$$

$$\sigma_C = \sum_{i,j=1}^N I_C(i,j) \quad (7)$$

In Equation (7), $I(i,j)$ is the intensity value at (i,j) in the crack map, where i and j both go from 1 to N because each cell is square. These values are summed across the entire cell, which gives the total amount of cracks in that cell, C .

$$\mu_{IA} = \frac{1}{M} \sum_{i,j=1}^M \sum_{i,j=1}^N I_C(i,j) \quad (8)$$

In Equation (8), μ_{IA} represents the average intensity value of each cell, C , across the entirety of the inspection area, IA , where M is the number of cells in the inspection area.

$$m_{IA} = \max(\sigma_1, \sigma_2, \dots, \sigma_C) \quad (9)$$

In Equation (9), it can be seen that m_{IA} is the maximum amount of cracks present in a cell in the inspection area. Using Equation (6) allows each cell to be represented in terms of its crack density with respect to the rest of the cells in the inspection area. The value of d is rounded to yield a binary decision on whether the ER sensor should be deployed in that cell. An example of the ER deployment map that is generated by the sensor fusion process can be seen in Fig. 8. In the provided example, it is easy to see that the inspection time saved by the proposed method is cost-effective as it saves 72 percent of the time spent deploying the ER sensors. An example inspection environment can be seen in Fig. 7.

IV. CONCLUSION AND FUTURE WORK

In this paper, we present a multi-functional inspection robot. Our robot is equipped with multiple NDE sensors associated with the developed fusion algorithm, which enables the robot to perform only necessary inspection methods in certain areas in order to reduce inspection time. Our robot was deployed to inspect several parking garages and concrete decks on UNR's campus. In the future, the robotic system can be deployed at more test sites in an attempt to quantify the impact and possible savings that the proposed sensor fusion method may have. The robot can be also deployed to inspect other civil infrastructures such as airport runways, seaport decks, bridge decks, etc. We plan to vigorously

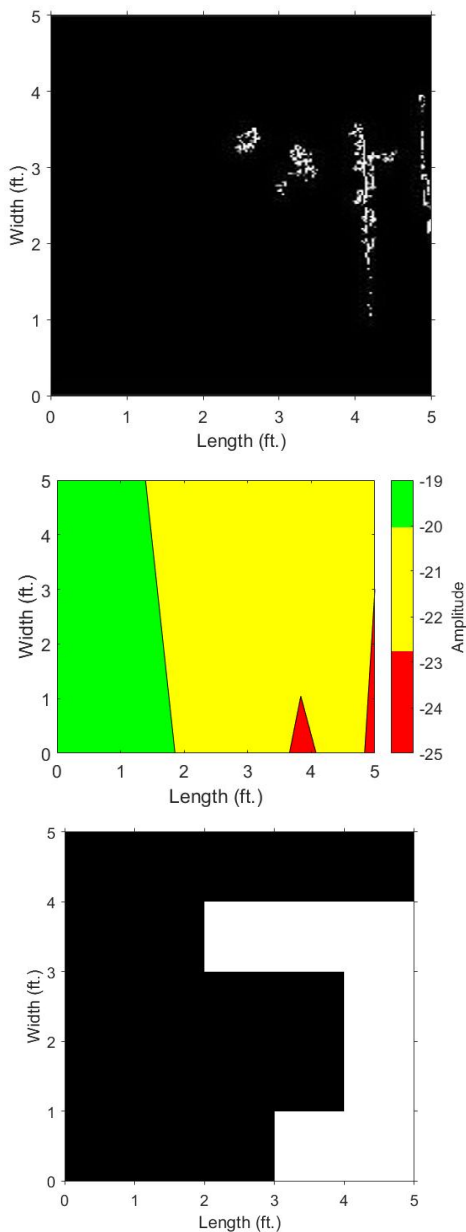


Fig. 8: A snapshot of the crack map (top), as well as a corresponding snapshot of the condition map (middle) and ER map resulting from the sensor fusion process (bottom). The white areas in the bottom image will be inspected further by the robot by using the ER sensor and the black areas will not.

conduct field testings to further evaluate and improve the robot's performance.

REFERENCES

[1] "Failure to act report - closing the infrastructure investment gap for america's economic future," American Society of Civil Engineerings, 2016.

[2] H. Furuta, T. Kameda, Y. Fukuda, and D. M. Frangopol, "Life-cycle cost analysis for infrastructure systems: life-cycle cost vs. safety level vs. service life," in *Life-cycle performance of deteriorating structures: Assessment, design and management*, 2004, pp. 19–25.

[3] T. D. Le, S. Gibb, N. H. Pham, H. M. La, L. Falk, and T. Berendsen, "Autonomous robotic system using non-destructive evaluation methods

for bridge deck inspection," in *Robotics and Automation (ICRA), 2017 IEEE International Conference on*. IEEE, 2017.

[4] R. S. Lim, H. M. La, and W. Sheng, "A robotic crack inspection and mapping system for bridge deck maintenance," *IEEE Transactions on Automation Science and Engineering*, vol. 11, no. 2, pp. 367–378, 2014.

[5] N. Gucunski, S. H. Kee, H. M. La, B. Basily, A. Maher, and H. Ghasemi, "Implementation of a fully autonomous platform for assessment of concrete bridge decks rabbit," *Structures Congress, April 23-25, 2015, Portland, Oregon, USA*, pp. 367–378, 2015.

[6] H. M. La, N. Gucunski, K. Dana, and S.-H. Kee, "Development of an autonomous bridge deck inspection robotic system," *Journal of Field Robotics*, 2017.

[7] H. M. La, N. Gucunski, S. H. Kee, and L. V. Nguyen, "Visual and acoustic data analysis for the bridge deck inspection robotic system," *The 31st International Symposium on Automation and Robotics in Construction and Mining (ISARC), Sydney, Australia*, pp. 50 – 57, 2014.

[8] H. M. La, N. Gucunski, S.-H. Kee, and L. V. Nguyen, "Data analysis and visualization for the bridge deck inspection and evaluation robotic system," *Visualization in Engineering*, vol. 3, no. 1, p. 6, Feb 2015. [Online]. Available: <https://doi.org/10.1186/s40327-015-0017-3>

[9] K. Dinh, N. Gucunski, J. Y. Kim, T. Duong, and H. M. La, "Attenuation-based methodology for condition assessment of concrete bridge decks using gpr," in *The 32st International Symposium on Automation and Robotics in Construction and Mining (ISARC), Oulu, Finland, June 15-18 2015*, pp. 1–8.

[10] H. M. La, R. S. Lim, B. B. Basily, N. Gucunski, J. Yi, A. Maher, F. A. Romero, and H. Parvardeh, "Mechatronic systems design for an autonomous robotic system for high-efficiency bridge deck inspection and evaluation," *IEEE/ASME Transactions on Mechatronics*, vol. 18, no. 6, pp. 1655–1664, 2013.

[11] H. M. La, N. Gucunski, S.-H. Kee, J. Yi, T. Senlet, and L. Nguyen, "Autonomous robotic system for bridge deck data collection and analysis." IEEE, 2014, pp. 1950–1955.

[12] M. Bloesch, S. Omari, M. Hutter, and R. Siegwart, "Robust visual inertial odometry using a direct ekf-based approach," in *Intelligent Robots and Systems (IROS), 2015 IEEE/RSJ International Conference on*. IEEE, 2015, pp. 298–304.

[13] H. M. La, R. S. Lim, B. Basily, N. Gucunski, J. Yi, A. Maher, F. A. Romero, and H. Parvardeh, "Autonomous robotic system for high-efficiency non-destructive bridge deck inspection and evaluation," in *2013 IEEE International Conference on Automation Science and Engineering (CASE)*, Aug 2013, pp. 1053–1058.

[14] T. H. Dinh, Q. P. Ha, and H. M. La, "Computer vision-based method for concrete crack detection," in *2016 14th International Conference on Control, Automation, Robotics and Vision (ICARCV)*, Nov 2016, pp. 1–6.

[15] P. Prasanna, K. J. Dana, N. Gucunski, B. B. Basily, H. M. La, R. S. Lim, and H. Parvardeh, "Automated crack detection on concrete bridges," *IEEE Transactions on Automation Science and Engineering*, vol. 13, no. 2, pp. 591–599, April 2016.

[16] J. Canny, "A computational approach to edge detection," *IEEE Transactions on Pattern Analysis and Machine Intelligence*, vol. PAMI-8, no. 6, pp. 679–698, Nov 1986.

[17] S. Gibb and H. M. La, *Automated Rebar Detection for Ground-Penetrating Radar*. Advances in Visual Computing: 12th International Symposium, ISVC 2016, Las Vegas, NV, USA, December 12-14, 2016, Proceedings, Part I: Springer International Publishing, 2016, pp. 815–824.

[18] G. Tanzmeister and S. Steyer, "Spatiotemporal alignment for low-level asynchronous data fusion with radar sensors in grid-based tracking and mapping," in *2016 IEEE International Conference on Multisensor Fusion and Integration for Intelligent Systems (MFI)*, Sept 2016, pp. 231–237.

[19] S. Larionova, L. Marques, and A. T. D. Almeida, "Multi-stage sensor fusion for landmine detection," in *2006 IEEE/RSJ International Conference on Intelligent Robots and Systems*, Oct 2006, pp. 2943–2948.

[20] R. Heideklang and P. Shokouhi, "Application of data fusion in non-destructive testing (ndt)," in *Proceedings of the 16th International Conference on Information Fusion*, July 2013, pp. 835–841.

[21] T. Khan, P. Ramuhalli, and S. C. Dass, "Particle-filter-based multi-sensor fusion for solving low-frequency electromagnetic nde inverse problems," *IEEE Transactions on Instrumentation and Measurement*, vol. 60, no. 6, pp. 2142–2153, June 2011.